The impact of explicit cloud boundary information on ice cloud microphysical property retrievals from infrared radiances

Steven J. Cooper, Tristan S. L'Ecuyer, and Graeme L. Stephens
Department of Atmospheric Science, Colorado State University, Fort Collins, Colorado, USA

Received 3 June 2002; revised 28 August 2002; accepted 8 September 2002; published 6 February 2003.

[1] Cirrus clouds have a profound impact on the radiation balance of the Earth–atmosphere system. Accurate representation of their radiative properties is critical to understanding climate and predicting climate change. This paper casts the split-window cirrus cloud retrieval technique in an optimal estimation framework facilitating direct inclusion of explicit cloud boundary information from complementary sensors as well as providing a suite of diagnostic tools for evaluating the dominant sources of uncertainty in all retrieved quantities. Errors in retrieved microphysical properties are used to determine the resulting errors in the calculation of global-scale radiative budgets. Uncertainties in optical depth and effective radius are found to diminish from ~45% and ~80%, respectively, in the absence of explicit cloud boundary information to ~15% and ~60% when accurate radar-based or lidar-based estimates are included. It is demonstrated that the improvements to cirrus cloud optical properties afforded by accurate cloud boundary information may lead to as much as a factor of 3 increase in the accuracy to which their impact on the Earth's radiative balance can be modeled. Colocated infrared radiances from the Moderate-Resolution Imaging Spectroradiometer (MODIS) instrument aboard the Earth Observing System (EOS) Aqua satellite and cloud radar observations from the CloudSat satellite will soon allow the retrieval presented here to be integrated into an operational retrieval of the vertical distribution of cloud properties on a global scale. *INDEX TERMS:* 0320 Atmospheric Composition and Structure: Cloud physics and chemistry; 3359 Meteorology and Atmospheric Dynamics: Radiative processes; 3360 Meteorology and Atmospheric Dynamics: Remote sensing; 3374 Meteorology and Atmospheric Dynamics: Tropical meteorology; 3394 Meteorology and Atmospheric Dynamics: Instruments and techniques; *KEYWORDS:* cirrus clouds, split-window, CloudSat, radiative fluxes

Citation: Cooper, S. J., T. S. L'Ecuyer, and G. L. Stephens, The impact of explicit cloud boundary information on ice cloud microphysical property retrievals from infrared radiances, *J. Geophys. Res.*, *108*(D3), 4107, doi:10.1029/2002JD002611, 2003.

1. Introduction

[2] The Earth's weather and climate is driven by the exchange of energy between the Sun, atmosphere, surface, and space. Cirrus clouds play a critical role in regulating this global energy balance through a combination of reflecting incoming solar radiation and absorbing and emitting long-wave radiation [*Liou*, 1986]. The relative magnitudes of these competing effects and their spatial and temporal variability is a crucial component modulating global atmospheric circulations, but the net effect of cirrus clouds on the global-scale and associated climate feedbacks are, at present, still poorly understood. Inadequate knowledge of the vertical distribution of cirrus cloud microphysical properties on a global-scale limits our ability to determine either the sign or the magnitude of their net radiative impact [*Stephens and Webster*, 1981; *Stephens et al.*, 1990]. As a result, significant uncertainties remain as to the net response and resulting feedback of cirrus clouds to global warming due to increasing CO_2 concentrations in the atmosphere [*Sassen*, 2002] and the role of cirrus clouds in the ocean–water vapor–convection feedback system [*Pierrehumbert*, 1995; *Lindzen et al.*, 2001; *Fu et al.*, 2002]. Furthermore, the role of cirrus in dehydrating the lower stratosphere and the resulting effects on stratospheric chemistry are yet undetermined [*Stephens*, 2002; *Rosenfield et al.*, 1998]. General circulation models (GCMs) may provide an invaluable tool for furthering our understanding of these and other processes in the cloud–radiation–climate system. Such models involve highly parameterized approximations to real-world physical processes and require accurate global observations of cirrus cloud microphysical properties to constrain and validate their results.

[3] Measuring the global distribution of cirrus cloud microphysical and optical properties has been a goal of numerous satellite missions such as the Television and Infrared Observations Satellite (TIROS) series, the Geostationary Operational Environmental Satellite (GOES) satellites, and the International Satellite Cloud Climatology Project (ISCCP) and continues to be a focal point for future endeavors including CloudSat and Cloud-Aerosol Lidar and Infrared Pathfinder Satellite Observations (CALIPSO) projects recently funded under the National Aeronautics and

0148-0227/03/2002JD002611$09.00

Space Administration (NASA) Earth System Science Pathfinder Project (ESSP). To make use of the resulting data, a suite of algorithms to infer a wide range of cirrus cloud properties has been developed to operate in concert with each of these satellites and, through major advancements in both instrumentation and remote sensing techniques, continuous progress has been made toward realizing the goal of globally mapping cirrus clouds. (The interested reader is referred to the study of *Miller et al.* [2000, Table 1] which summarizes a broad cross section of such algorithms.) Both the NASA Cloud and Earth Radiant Energy (CERES) and the Moderate-Resolution Imaging Spectroradiometer (MODIS) programs have developed and/or exploited these multispectral techniques to produce global distributions of cirrus properties and to investigate their effects on the Earth's climate [*King et al.*, 1992; *Wielicki et al.*, 1996]. In the spirit of these efforts, this paper presents an advanced version complete with error analysis of the algorithm commonly referred to as the split-window technique. It is not our intention to replace the work of these advanced programs but to demonstrate how the use of explicit cloud boundary information and the proper error characterization of retrieved cloud properties are important in determining uncertainties in related climate studies. Although we choose to focus on the split-window method, the physics underlying the other techniques could easily be incorporated into our algorithm and, in fact, we will show how this technique can be combined with ongoing research at Colorado State University (CSU) to provide a retrieval of the vertical distribution of cirrus cloud properties with complete error diagnostics for the satellites of the NASA ESSP mission.

[4] The split-window technique relies on differences in radiative properties for cloud particles at two wavelengths in the atmospheric window region of the infrared spectrum to estimate cloud optical depth and effective radius from satellite-observed brightness temperatures [*Inoue*, 1985; *Prabhakara et al.*, 1988]. An inherent shortcoming of the original implementations of the approach is that the retrieved parameters are heavily dependent upon an assumed cloud thermodynamic temperature. Traditionally, a lack of explicit cloud boundary information has resulted in significant biases in retrieved cloud properties [*Miller et al.*, 2000]. Through the use of an optimal estimation-based inversion [*Rodgers*, 1976, 1990; *Marks and Rodgers*, 1993], the algorithm introduced in the present work is capable of incorporating explicit cloud boundary information from complementary sensors such as spaceborne lidar or cloud radar to constrain cloud thermodynamic temperature in the algorithm.

[5] The optimal estimation approach to inversion and its application to the split-window technique will be introduced in the next section. A new two-layer radiative transfer model for relating cirrus cloud optical depth and effective radius to infrared radiances in an efficient and accurate manner is developed and evaluated in section 3. In section 4.1, the algorithm is evaluated through a series of synthetic retrievals designed to demonstrate the salient features of the approach as well as to characterize uncertainties in retrieved optical depth and effective radius as a function of the accuracy of cloud boundary information employed. In section 4.2, the algorithm is applied to infrared radiances from the Visible and Infrared Scanner (VIRS) aboard the Tropical Rainfall Measurement Mission (TRMM) satellite in conjunction with cloud boundaries from the Atmospheric Radiation Measurement (ARM) program's Tropical Western Pacific (TWP) Nauru Island site to evaluate its performance with cloud boundary information of varying accuracy. The implications of these results for climate study are addressed in section 4.3 and relevant results and possible extensions of the technique are discussed in section 5.

2. The Optimal Estimation Approach

[6] Ultimately, estimates provided by cloud optical property retrievals are needed to improve our understanding of the mechanisms by which clouds interact with solar and terrestrial radiation to help shape the Earth's climate. Such applications require extensive spatial and temporal coverage, special care to remove any sources of systematic errors in the retrieval method and rigorous estimates of the uncertainties in all products. Regrettably, this final requirement represents a significant shortcoming in many modern retrieval algorithms.

[7] The approach adopted here is based on the physical principles that underlie the method introduced by *Prabhakara et al.* [1988]. At the root of the method is the fact that ice particles on the order of 30 μm or smaller more efficiently absorb radiation at a wavelength of 12 μm than at 10.8 μm. As a result, cirrus clouds composed of small ice particles appear "colder" at 12 μm than at 10.8 μm. When examined at a variety of cirrus optical depths and effective radii, the relationship between $\Delta T_B = T_{B,10.8} - T_{B,12}$ and $T_{B,10.8}$ resembles an arch. The right foot of the arch corresponds to the clear-sky emitting temperature of the Earth while the left foot represents an optically thick cloud where $T_{B,10.8}$ and $T_{B,12}$ each approach the cloud thermodynamic temperature. Intermediate values provide information regarding the optical properties of the cloud. Theoretically derived relationships between ΔT_B and $T_{B,10.8}$ for a number of different cirrus clouds are illustrated in Figure 1. (These arches and all subsequent analyses are based on a TRMM satellite viewing angle of 45°.) Accurate specification of cloud temperature, as well as emitting temperature of the clear sky, is clearly critical for a good retrieval. For a given ΔT_B and $T_{B,10.8}$ measurement, the split-window technique yields a different effective radius and optical depth for each cloud temperature. It should be noted from Figure 1 that the working range of the retrieval is limited to 10.8 μm optical depths up to about 2.0 and effective radii from about 5 to 25 μm, depending on the precise cloud thermodynamic temperature. Uncertainties in the clear-sky emitting temperature also make estimates of optical depths less than about 0.2 dubious.

[8] The fact that the method is rooted in the interaction of cloud particles with infrared radiation, however, means that it can be applied without modification during the daytime and at night and is thus well suited for application to satellite platforms required for near-global observations. In the present study, as opposed to look-up tables that are susceptible to biases introduced by the required assumption of cloud thermodynamic temperature and often lack rigorous uncertainty estimates, we adopt an optimal estimation implementation of the retrieval method [*Rodgers*, 1976, 1990; *Marks and Rodgers*, 1993]. The technique provides a framework for making use of the accuracy in the measure-

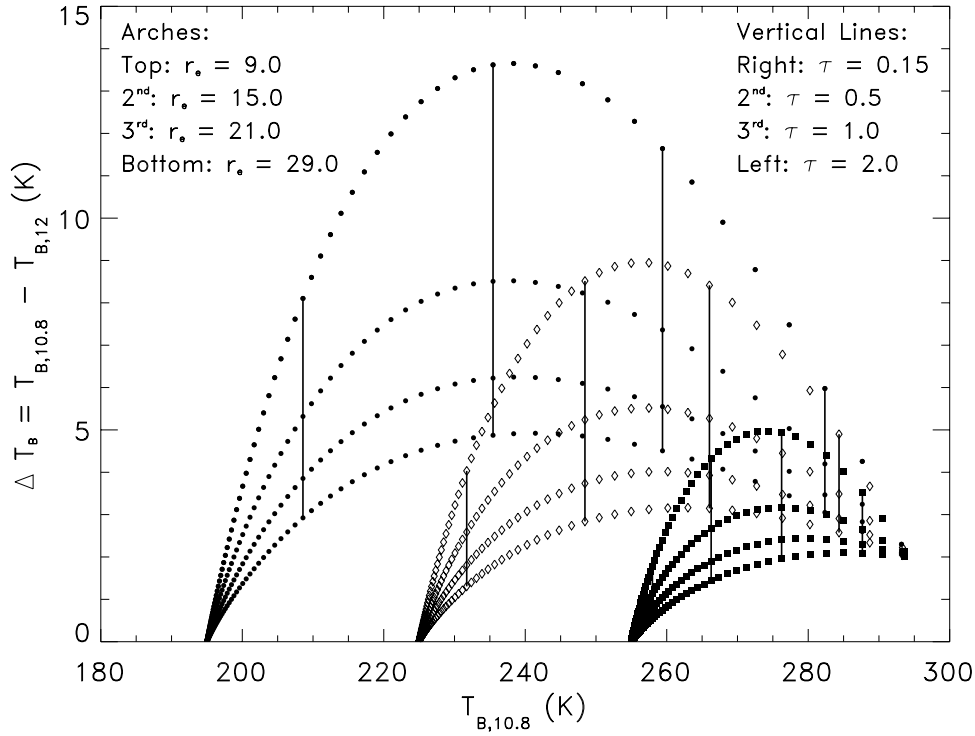

Figure 1. Relationship between ΔT_B and $T_{B,10.8}$ for a number of cirrus clouds with 10.8 μm optical depths ranging from 0 to 4 and effective radii ranging from 9 to 29 μm. Clouds with emitting temperatures of 195 K (filled circles), 225 K (open diamonds), and 255 K (filled squares) are modeled.

ments and physical model to determine the strength of their influence on the retrieval and for propagating these errors through the estimation process to estimate uncertainties in all retrieved parameters. Furthermore, biases introduced by the assumption of a cloud thermodynamic temperature are mitigated by the introduction of cloud temperature as a variable parameter in the retrieval. While these benefits may not be exclusive to the optimal estimation approach, it provides the benefit of an elegant framework that is straightforward to implement and is well suited to combining information from multiple sensors provided the added computational cost is not prohibitive.

[9] Recent studies by *Engelen and Stephens* [1997, 1999], *Miller et al.* [2000], *Austin and Stephens* [2001], *Stephens et al.* [2001b], and *L'Ecuyer and Stephens* [2002] have applied the optimal estimation technique to retrievals of ozone, water vapor, cloud properties, rainfall, and aerosols from a combination of lidar, radar, and passive measurements at visible, infrared, and microwave wavelengths. Many of the mathematical details of the approach can be found in these references but a short summary is provided here for completeness. Letting $\hat{\mathbf{x}}$ denote the vector of cloud properties to be retrieved, the optimal estimation technique consists of minimizing a combination of the variance between the set of observations, $\mathbf{y}$, and a corresponding set of simulated measurements, $F(\hat{\mathbf{x}})$, and that between $\hat{\mathbf{x}}$ and a suitable a priori guess, $\mathbf{x}_a$. Assuming Gaussian statistics, this is accomplished by minimizing the scalar cost function,

$$\Phi(\hat{\mathbf{x}}, \mathbf{y}, \mathbf{x}_a) = (\mathbf{y} - F(\hat{\mathbf{x}}))^T \mathbf{S}_y^{-1} (\mathbf{y} - F(\hat{\mathbf{x}})) + (\hat{\mathbf{x}} - \mathbf{x}_a)^T \mathbf{S}_a^{-1} (\hat{\mathbf{x}} - \mathbf{x}_a) \quad (1)$$

with respect to $\mathbf{x}$. (In principle, any non-Gaussian statistics could be invoked). *Rodgers* [2000], however, notes that according to the Principle of Maximum Entropy, the Gaussian distribution is the most appropriate if only a mean and variance is known. Alternative distributions, unless known and rigorously justifiable, add spurious information to the retrieval and biases estimation of the most probable solution.) F denotes the physical model relating the cloud parameters to the observations called the "forward model," $\mathbf{S}_a$ is the a priori error covariance matrix, and $\mathbf{S}_y$ is the measurement error covariance matrix consisting of a combination of observation and the forward model uncertainties.

[10] The values of $\hat{\mathbf{x}}$ for which (1) is minimum can be found by Newtonian iteration via

$$\hat{\mathbf{x}}^{i+1} - \hat{\mathbf{x}}^i = \mathbf{S}_x \left[\mathbf{K}_i^T \mathbf{S}_y^{-1} \left(\mathbf{y} - \mathrm{F}(\hat{\mathbf{x}}^i) \right) + \mathbf{S}_a^{-1} \left(\mathbf{x}_a - \hat{\mathbf{x}}^i \right) \right] \quad (2)$$

where

$$\mathbf{S}_x = \left(\mathbf{S}_a^{-1} + \mathbf{K}_i^T \mathbf{S}_y^{-1} \mathbf{K}_i \right)^{-1} \quad (3)$$

is the error covariance matrix of the estimated parameters accounting for uncertainties in the forward model, measurements, and a priori data. The Kernel or weighting function matrix, $\mathbf{K}$, is the Jacobian of the forward model with respect to the retrieval vector, with elements given by

$$K_{jk} = \frac{\partial F_j}{\partial x_k} \quad (4)$$

The iteration proceeds until such time as the covariance-weighted mean difference between successive estimates is much less than the number of independent variables in the retrieval vector, i.e.,

$$\left(\hat{\mathbf{x}}^{i+1} - \hat{\mathbf{x}}^{i}\right)\mathbf{S}_y^{-1}\left(\hat{\mathbf{x}}^{i+1} - \hat{\mathbf{x}}^{i}\right) \ll N_x \tag{5}$$

[11] Among the advantages of this approach is the fact that it allows the algorithm developer complete flexibility regarding the choice of retrieval parameters and observations. In principle any set of measurements can be used to retrieve any set of parameters provided one can define a forward model to suitably represent the relationship between them and assign uncertainties to this model and the observations themselves. Making use of this flexibility, we adopt a retrieval consisting of not only effective radius, r_e, and optical depth, τ, but which also includes cloud thermodynamic temperature, T_c, as an adjustable retrieval parameter. At the same time we add an estimate of cloud thermodynamic temperature to the measurement vector, in part to avoid defining a grossly under constrained problem but also to provide a framework for including direct estimates of T_c from complementary sensors. At first, it may seem strange to include T_c as both an observation and a retrieval parameter but it merely affords us the luxury of using T_c as a soft constraint on the retrieval. Ultimately the strength of this constraint is determined by the accuracy to which cloud temperature can be determined, σ_{Tc}. By including T_c in both the observation and retrieval vectors, its role smoothly varies from a purely retrieved result when σ_{Tc} is large to a pure observation that constrains the retrieval when σ_{Tc} is small. At intermediate accuracies, T_c constrains the retrieval to search for solutions along arches corresponding to the observed cloud thermodynamic temperature but can be modified within its error bounds in cases where the combination of $T_{B,10.8}$, T_c, and ΔT_B are unphysical (e.g., if ΔT_B is large but $T_{B,10.8} \sim T_c$, the T_c estimate must be too high). It will be shown that this approach leads to a significantly greater overall consistency between retrieval products and observations particularly in cases where at most a rough estimate of T_c is available.

3. The Forward Model

[12] Application of (3) requires a physical model for mapping $\mathbf{x} = (\tau, r_e, T_c)$ into the observation space defined by $\mathbf{y} = (T_{B,10.8}, \Delta T_B, T_c)$ and a rigorous assessment of its uncertainty.

3.1. Radiative Transfer Model

[13] A two-layer radiative transfer model has been developed to simulate the 10.8 and 12.0 μm radiances as observed by a satellite as a function of cloud optical depth, effective radius, and cloud temperature. The model consists of an isothermal cirrus cloud overlying an emitting clear-sky layer and assumes that scattering is negligible at infrared wavelengths. (This assumption requires some justification. Ice particles of radii 10–50 μm which may be found in cirrus clouds scatter approximately as much IR radiation as they absorb. When an ensemble of these particles are modeled in a typical cirrus cloud, however, *Stephens* [1980] showed that they lead to a total IR reflectance of only about 5% or 10 W m^{-2}. While this may be significant in some applications, errors introduced by the simple radiative transfer model will be far greater in the present study.) Under these assumptions, the observed radiance at the top of the atmosphere (TOA) is the sum of clear-sky emission transmitted through the cirrus cloud plus emission by the cloud itself,

$$I_{obs} = I_{cs}e^{-\tau/\mu} + B(T_c)\left[1 - e^{-\tau/\mu}\right] \tag{6}$$

where τ is cloud optical depth, μ is the cosine of the solar zenith angle, and $B(T_c)$ is the Planck blackbody function for cloud temperature T_c.

[14] The size and shape of the constituent cloud particles enters the model through their influence on optical depth. For a monodispersed distribution of spherical particles of radius r, the optical depth at a wavelength, λ, is

$$\tau_\lambda = \pi N_0 r^2 Q_{abs,\lambda}\Delta z \tag{7}$$

where N_0 is the number of particles per unit volume, $Q_{abs,\lambda}$ is the absorption efficiency, and Δz is the geometric thickness of the cloud. The ratio of the optical depths at 10.8 and 12.0 μm is simply the ratio of the absorption efficiencies at the two wavelengths, which are estimated using an anomalous diffraction theory approximation developed by *Flatau* [1992] for spherical particles,

$$Q_{abs} \approx 2\left[\frac{1}{2} + \frac{e^{-4\chi\kappa}}{4\chi\kappa} + \frac{e^{-4\chi\kappa} - 1}{(4\chi\kappa)^2}\right] \tag{8}$$

κ is the imaginary part of the refractive index and $\chi = 2\pi r/\lambda$ is the size parameter. The accuracy of the ADT approximation relative to explicit Mie calculations for spherical particles is assessed by *Flatau* [1992] and leads to errors of less than 5% at 10.8 and 12.0 μm. This model is easily extended to a polydispersed distribution, n(r), by direct integration.

$$\frac{\tau_{12.0}}{\tau_{10.8}} = \frac{\int \pi Q_{abs,12.0}(r) r^2 n(r) dr}{\int \pi Q_{abs,10.8}(r) r^2 n(r) dr} \tag{9}$$

For the retrieval, a modified gamma distribution of spherical particles with variance equal to 2.0 is used [*Dowling and Radke*, 1990]. Hereafter this distribution will be referred to as the model distribution for simplicity. The impact of these assumptions will be examined in detail in the following section to estimate an appropriate forward model error covariance matrix for use in the retrieval. It should be noted that, while (8) and (9) hold only for spherical particles, the ratio of the optical depths for nonspherical particles can be estimated through more advanced methods, such as the finite difference time domain method (FDTD) [*Yang et al.*, 2001] facilitating modifications to particle shape if necessary.

3.2. Model Calibration

[15] Equations (6)–(9) constitute a simple, complete model governing the transmission of radiation through a cirrus cloud from which 10.8 and 12.0 μm brightness temperatures can be evaluated for any combination of cloud particle size distribution, optical depth, and cloud temper-

ature. When compared to a more sophisticated radiative transfer model developed by *Deeter and Evans* [1998] (hereafter referred to as the DE model), differences emerge. Analysis of model differences for a variety of cases spanning the range of optical depths and effective radii over which the retrieval is to be applied suggest that they are functions of cloud temperature, optical depth, and effective radius. Since for certain cloud property combinations $T_{B,10.8}$ differences between models can be nearly 5 K, a correction was developed to improve agreement between the present and DE models to remove systematic biases from our results. Details regarding the correction can be found in Appendix A. With the correction, the simple two-layer model can be employed as opposed to the DE model with minimal loss of accuracy affording an increase in computation speed of approximately a factor of 100. This increase in speed is particularly important in the optimal estimation framework. Typically, five iterations are required to reach convergence at any pixel, with each iteration invoking seven executions of the forward model. Thus, the forward model is called an average of 35 times per pixel. The corrected model yields an accurate and computationally efficient solution that is, therefore, essential for processing the large amounts of satellite data required for global applications of the retrieval.

3.3. Error Covariance Matrices

[16] Proper estimation of error covariance matrices is critical to the success of any optimal estimation retrieval. In the absence of additional information, the a priori guess is limited to a rough estimate of the climatological mean effective radius, optical depth, and emitting temperature of typical cirrus clouds. To account for the lack of quantitative information in the a priori guess, its covariance matrix is assigned to represent the full range of the cirrus properties for which the retrieval is applicable and is therefore reasonably well specified. Calibration errors in VIRS satellite measurements of brightness temperatures will be assumed to range from 1 K for a cirrus cloud emitting at 220 K to 1.5 K for cloud emitting at 275 K [*Lyu et al.*, 2000].

[17] Determining forward model errors is the most challenging task and is the primary focus of this section. Since the cloud temperature error in the model is variable by design, we only need determine the error in I_{cs}, $T_{B,10.8}$, and ΔT_B associated with the forward model. The effects of I_{cs} on retrieved parameters are significantly smaller than those effects of cloud temperature, so I_{cs} is simply treated as a constant derived from the DE model employing a McClatchey Tropical Atmosphere [*McClatchey et al.*, 1972]. For an operational retrieval, however, a rigorous pixel by pixel estimation of clear-sky emitting temperature with error estimates should be made for accuracy.

[18] Based on the discussion above, the forward model determines the theoretical $T_{B,10.8}$ and ΔT_B observed by a satellite for a given effective radius, optical depth, and cloud temperature. The model, however, is based on a set of assumptions that, if changed, can yield substantially different results. The most prominent of these assumptions is the choice of the ''model distribution,'' a modified gamma cloud particle distribution of ice spheres with variance equal to two. If the cloud particle size distribution or particle habit are changed, then the absorption characteristics at both 10.8 and 12.0 μm change, leading to a new $T_{B,10.8}$ and ΔT_B. To estimate the expected error in model results associated with choice of distribution and habit, a variety of cloud particle size distributions each with the same effective radius for both ice spheres and hexagonal columns have been substituted into the model and the resulting $T_{B,10.8}$ and ΔT_B compared over a wide range of optical depths and effective radii.

[19] Five different modified gamma and four different lognormal cloud particle size distributions for both ice spheres and hexagonal columns were used. The modified gamma distribution is of the form

$$n(D) = N_t \frac{1}{\Gamma(\nu)} \left(\frac{D}{D_n}\right)^{\nu-1} \frac{1}{D_n} e^{-D/D_n} \tag{10}$$

where $n(D)$ is the number of ice crystals of size D, N_t is the number concentration, D_n is the characteristic diameter, and ν is the distribution variance [*Stephens*, 1994]. The lognormal distribution is of the form

$$n(D) = \frac{1}{D \ln \sigma_g (2\pi)^{0.5}} \exp\left[\frac{\left(\ln D - \ln D_g\right)^2}{2\left(\ln \sigma_g\right)^2}\right] \tag{11}$$

where D_g is the geometric mean diameter and σ_g is the geometric standard deviation [*Reist*, 1993]. Figure 2 shows each of the distributions generated using (10) and (11) for an effective radius of 20 μm, where effective radius is defined as

$$r_e = \frac{\int_a^b n(r) r^3 dr}{\int_a^b n(r) r^2 dr} \tag{12}$$

where a and b are chosen such that the integrals converge.

[20] For spherical particles, the ADT approximation in (8) was used to determine the ratio of optical depths at 10.8 and 12.0 μm for the distribution. Differences in this ratio of optical depths between the test distributions and the model distribution determines the error in the ΔT_B value while the difference in the total optical depth between the two distributions determines the error in $T_{B,10.8}$. For hexagonal crystals, explicit calculations of the absorption efficiencies at 10.8 and 12.0 μm as a function of crystal size from the study of *Yang et al.* [2001] are used. Due to current limitations in the understanding of absorption characteristics of other crystal habits at infrared wavelengths, estimation of model error incurred as a result of particle shape is limited to these hexagonal crystals. To facilitate comparisons between spherical and hexagonal crystals, all particles are represented as equivalent spherical distribution in which both the area and volume of the distribution is conserved [*Francis et al.*, 1994; *Mitchell and Arnott*, 1994; *Grenfell and Warren*, 1999; *Yang et al.*, 2001].

[21] Theoretical relationships between ΔT_B and $T_{B,10.8}$ (hereafter referred to as ''arch curves'') generated for the cloud particle 2 of Figure 2 for both ice spheres and hexagonal crystals at a cloud temperature of 220 K are shown in Figure 3. The top set of curves shows the variability associated with different spherical distributions while the bottom set corresponds to hexagon column dis-

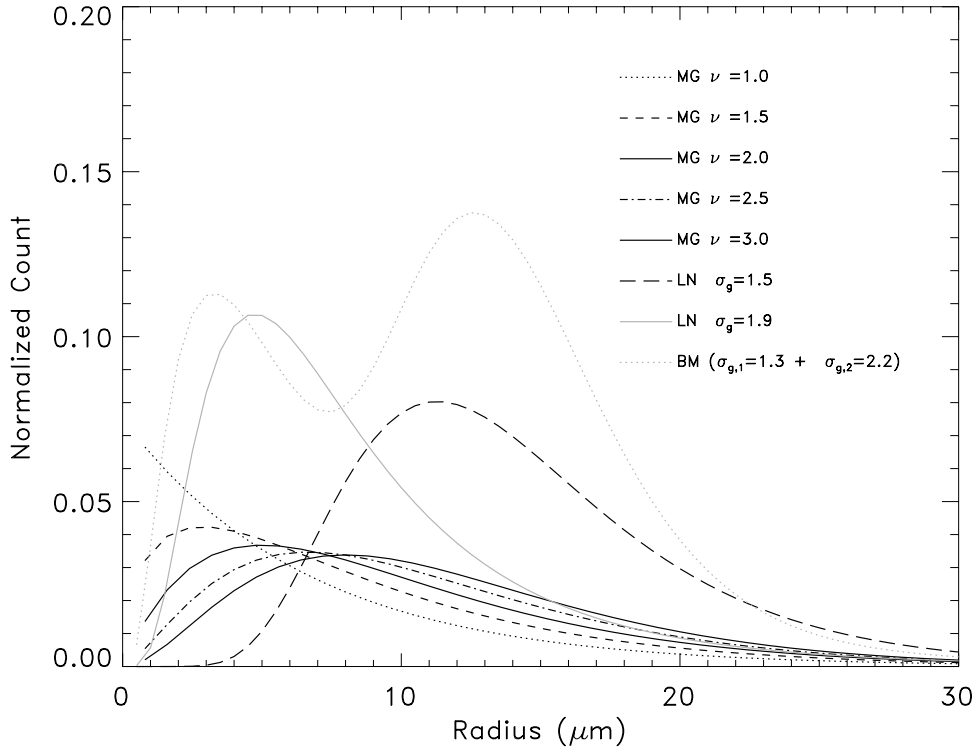

Figure 2. Size distributions used in estimating forward model error covariance matrices. Modified gamma distributions are designated MG, lognormal distributions LN, and the bimodal distribution, which is simply the addition of 2 lognormal distributions, BM. The effective radius of each distribution is 20 μm.

tributions. Clearly, the variance between the two crystal habits exceeds the variance between size distributions with the same habit, consistent with the results of *Stephens et al.* [1990]. Thus, we conclude that the variance between crystal habits dominates the measurement and forward model covariance matrix. Unfortunately, this variance is difficult to assess exactly given the lack of absorption data for other crystal habits (e.g., plates, rosettes, aggregates, etc.) and the generally complex mix of ice crystals observed in real clouds. Given that polycrystals scatter and absorb more like spheres, it is reasonable to assume that the difference between hexagonal columns and spherical crystals represents a pessimistic estimate of habit error. Thus, we might assume that an order of magnitude estimate of forward model uncertainties based on Figure 3 are representative of the maximum one would encounter using all possible habits. This assumption is supported by *Parol et al.* [1991] who calculated the ratio of optical depths at 10.8 and 12.0 μm for infinite cylinders and obtained similar results.

[22] For the case illustrated in Figure 3, the difference in $T_{B,10.8}$ between the model distribution and hexagonal crystals is about 3 K when averaged over the working range of the optical depth retrieval at 10.8 μm. The average difference in ΔT_B between the model distribution and hexagonal crystals is about 2 K over the same range. The errors depend weakly on both effective radius and cloud thermodynamic temperature since the magnitudes of both ΔT_B and $T_{B,10.8}$ depend on the choice of r_e and T_c. Smaller effective radii tend to yield a larger difference in ΔT_B but a smaller difference in $T_{B,10.8}$ between habits. Furthermore, the colder the cloud, the greater the absolute error in ΔT_B. As a result, the case shown, corresponding to a cold cloud at 220 K with an effective radius of 20 μm, is representative of conditions under which the errors are larger than average. Based on this argument and the estimates of VIRS calibration error, standard deviations of 1.5 and 2.5 K for ΔT_B and $T_{B,10.8}$, respectively, are used for the diagonal elements of the measurement covariance matrix in the retrieval. In an operational retrieval, these values should be determined as a function of cloud thermodynamic temperature and effective radius for a more rigorous result. For completeness, several different choices of ΔT_B and $T_{B,10.8}$ error are used in the synthetic retrievals that follow to illustrate how the retrieval is affected by the forward model accuracy.

[23] As ΔT_B and $T_{B,10.8}$ are clearly correlated, it is also important to include some estimate of the off-diagonal elements of the measurement error covariance matrix. Taking the average difference between the model distribution and each of the test distributions described above for each of the variables, the covariance between ΔT_B and $T_{B,10.8}$ was found to be -3.5 when normalized by the appropriate standard deviations. Again, differences in habit dominate the magnitude and sign of the covariance. The correlation is negative since a decrease in ΔT_B relative to the model distribution is generally accompanied by a corresponding increase in $T_{B,10.8}$. Physically, this is a manifestation of the fact that hexagonal crystals have smaller absorption cross sections at both 10.8 and 12 μm than equivalent volume to area spheres, reducing the ice cloud signal in both $T_{B,10.8}$

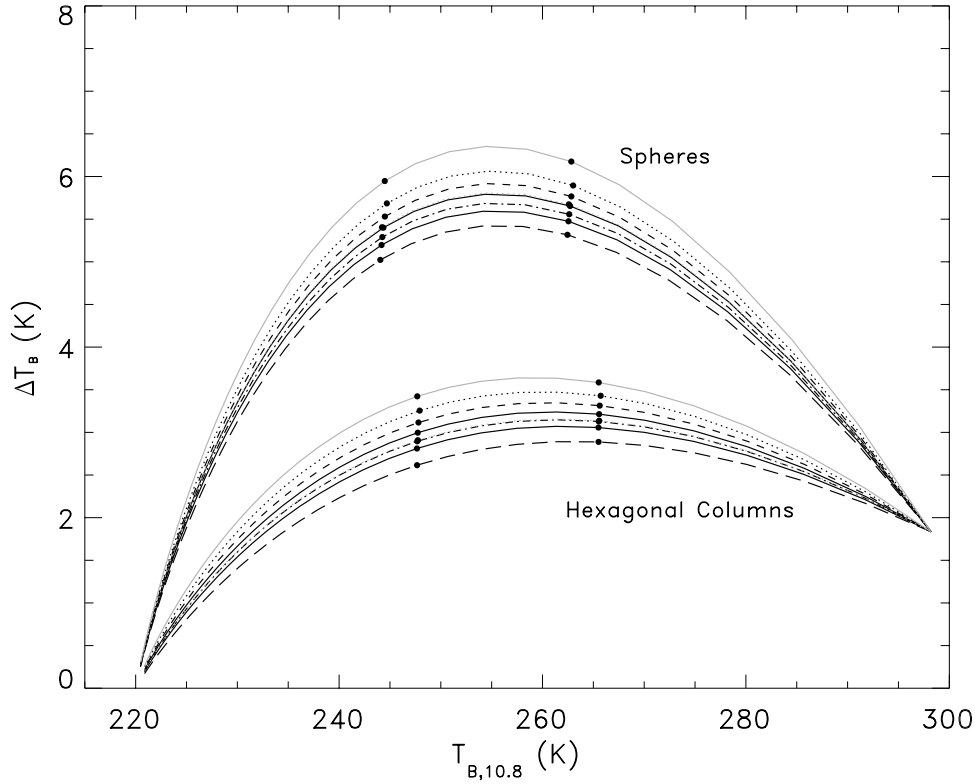

Figure 3. $\Delta T_B - T_{B,10.8}$ relationships for a set of 220 K ice clouds. The upper set of curves correspond to each of the distributions in Figure 2 assuming spherical particles while the lower set corresponds to an equivalent set of of hexagonal columns. The set of closed circles on the right corresponds to a model distribution optical depth of 0.5 at 10.8 μm, while those on the left to an optical depth of 1.0 at 10.8 μm.

and ΔT_B. Thus more radiation from below the cloud emerges at TOA leading to an increase in $T_{B,10.8}$ and $T_{B,12}$ and a decrease in the difference between them.

[24] It should be noted that there exist a number of additional sources of uncertainty that have not been addressed here, such as errors due to the cloud three-dimensional structure and subpixel variability. Evaluation of the impact of these error sources requires a more rigorous treatment and are topics of ongoing research.

4. Algorithm Evaluation

[25] The performance of the algorithm has been tested using a combination of synthetic retrievals and real-world retrievals making use of cloud boundary measurements from the ARM program's TWP site at Nauru Island. While synthetic retrievals may be somewhat biased by the fact that similar assumptions are often made in both forward and inverse calculations, they provide an invaluable tool for testing the behavior of the algorithm under controlled conditions. These studies must, however, be complemented with applications involving real observations. Selected results from both types of studies will be discussed below.

4.1. Synthetic Retrievals

[26] A set of effective radii, optical depths, and cloud thermodynamic temperatures representative of typical cirrus clouds were applied in the two-layer model to produce synthetic "observations" with which to test the algorithm. Random errors were simulated by adding Gaussian noise directly proportional to the standard deviation used in the measurement error covariance matrix to each of the synthesized $T_{B,10.8}$, ΔT_B, and cloud temperature measurements. This perturbed measurement vector was then run through the optimal estimation retrieval to assess the quality of the retrieved optical depth and effective radius. Each measurement vector was randomly perturbed 5000 times to produce a statistically significant distribution of errors about the measurements.

[27] Figures 4 and 5 show the percentage error in retrieved optical depth and effective radius, respectively, for a cloud with a 10.8 μm optical depth of 0.8, an effective radius of 14 μm, and an emitting temperature of 225 K. Retrieval error is defined as the standard deviation of the retrievals divided by the expected mean expressed as a percent, $\sigma_i = \sqrt{(\mathbf{S_x})_{ii}}/x^*_{truth}100$, and is plotted as a function of error in the cloud temperature measurement for three sets of $T_{B,10.8}$ and ΔT_B error assumptions. These figures illustrate retrieval performance for a given measurement with inherent random error. Gaussian statistics dictate that 68 percent of the randomly perturbed retrievals fall within one standard deviation from the retrieved mean. Clearly the lower the error in T_c estimate, the higher the probability of retrieving a value close to the truth. For fixed error in T_c, better estimates of $T_{B,10.8}$ and ΔT_B also yield better retrieval results. Note that the shapes of the curves, however, are

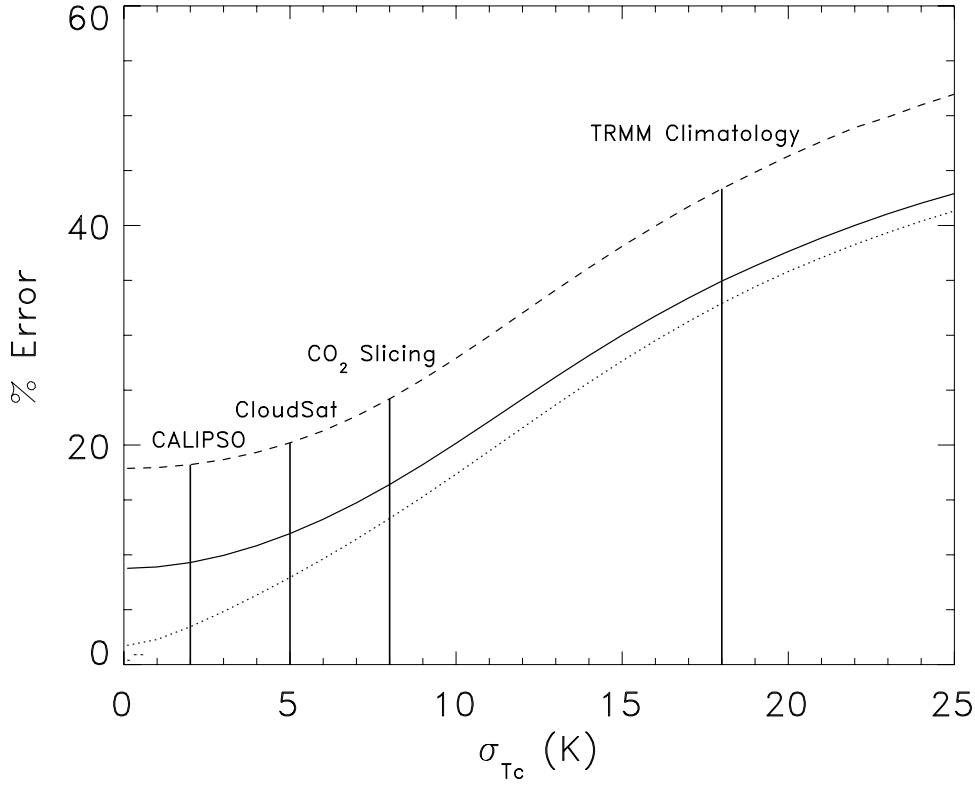

Figure 4. Error statistics for synthetic retrievals of 10.8 μm optical depth for different covariance matrix assumptions. The dotted line corresponds to a $\sigma_{\Delta T_B}$ of 0.5 K and a $\sigma_{T_{B,10.8}}$ of 0.5 K. The solid line to 1.5 and 2.5 K and the dashed line to 3.0 and 5.0 K. The vertical lines represent the estimated error in cloud thermodynamic temperature determined using a variety of techniques. Results are for an optical depth of 0.8, an effective radius of 14 μm, and cloud thermodynamic temperature of 225 K.

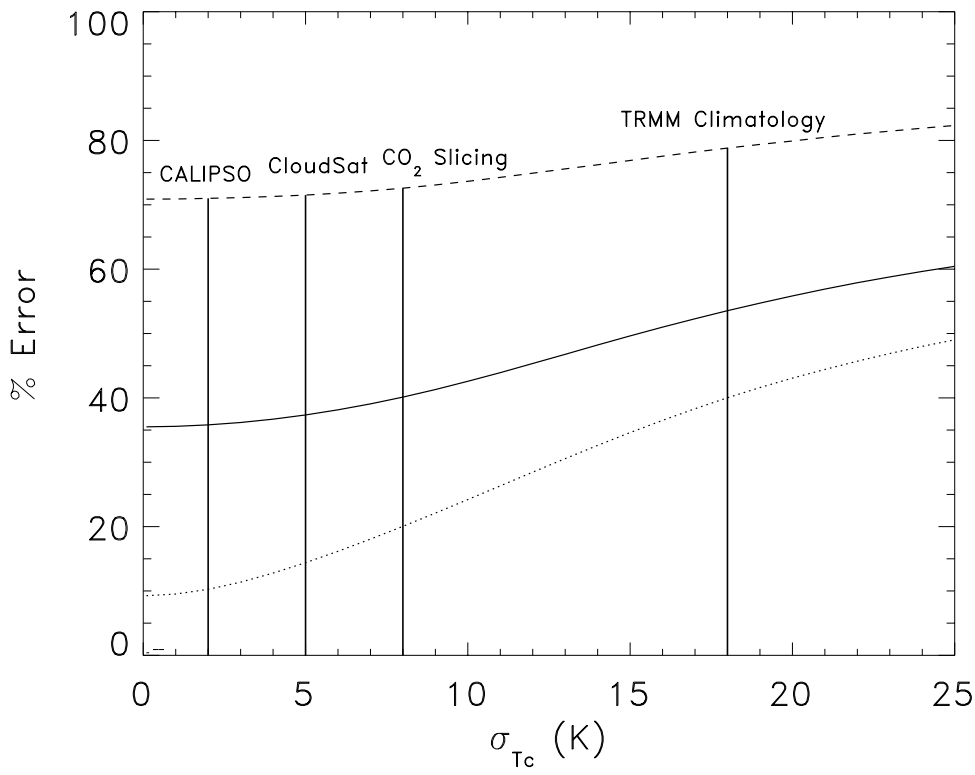

Figure 5. As in Figure 4 but for retrievals of effective radius.

different for the optical depth and effective radius cases. The optical depth retrievals show much greater sensitivity to T_c measurement error than effective radius. Furthermore, effective radii exhibit substantially larger relative errors than optical depths.

[28] Also plotted on the figures are vertical lines corresponding to estimated accuracies in different techniques for determining T_c. Active systems such as, lidar and radar, for example, can be used to determine cloud boundaries that can, in turn, be related to cloud temperature through the assumption of an atmospheric temperature profile. Uncertainties in these cases arise from a combination of the vertical resolution of the instrument and deviations from the assumed vertical temperature profile. Uncertainties in lidar-based and radar-based estimates of T_c are estimated to be 2 and 5 K, respectively, based on an expected accuracy of 2 K in atmospheric temperature profiles from numerical weather prediction models [*Eyre et al.*, 1993] and assuming vertical resolutions of 30 and 500 m characteristic of the CALIPSO lidar and the CloudSat cloud profiling radar (CPR). (See CloudSat and CALIPSO webpages for documentation of vertical resolutions: www.cloudsat.atmos.colostate.edu and www.calipso.larc.nasa.gov/instrument.html.)

[29] Passive techniques such as CO_2 slicing can also be used to estimate cloud top pressure which can then be related to cloud temperature, again through assumption of a temperature profile. Based on the work of *Menzel et al.* [1992] and *Baum and Wielicki* [1994], a CO_2 slicing-derived cloud top pressure of 300 mb has a maximum random error of 50 mb. This translates to an error in cloud thermodynamic temperature of 8 K.

[30] One alternative to explicitly measuring cloud boundary information is to resort to a reasonable climatological mean value. In the present study a climatology of cloud thermodynamic temperature is made by matching infrared radiances and precipitation information from the TRMM satellite. As discussed in the next section, uncertainties in the resulting "TRMM climatologies" are estimated to be about 18 K.

[31] Figures 4 and 5 show only statistics for those retrievals that converged to physically realistic values of effective radius, optical depth, and cloud thermodynamic temperature for all three pairs of $\sigma_{\Delta T_B}$ and $\sigma T_{B,10.8}$. Table 1 lists the number of convergent cases out of the 5000 perturbations for each combination of measurement error. Since cases with large error are more likely to be nonconvergent, Figures 4 and 5 underestimate retrieval errors at high σ_{Tc} since the worst retrievals are all thrown out and not used in the statistics. To get a complete picture, the results from the number of nonconvergent pixels must be considered together with the results in Figures 4 and 5 as it is just as undesirable to have a nonconvergent retrieval as one with large uncertainty. It should also be noted that the standard deviations are not symmetric about truth, as the retrieved mean does not always converge to the expected mean. Large error covariance matrices, for example, result in a bias in the retrieval since it becomes more influenced by the assumed a priori guess.

[32] Table 1 also lists the mean effective radius, optical depth, and diagonal elements of the averaging kernel for all convergent retrievals. The averaging kernel can be loosely interpreted as the relative contribution of the measurements to the a priori guess in the retrieval [*Rodgers*, 1990]. Values near unity are desirable as they indicate a heavy weighting of the measurements while values near zero characterize a retrieval, which derives primarily from the a priori guess in which we have no confidence. Clearly, errors in retrieved optical depth and effective radius increase as σ_{Tc}, $\sigma_{T_{B,10.8}}$, and $\sigma_{\Delta TB}$ increase. These qualitative trends are to be expected and reflect the mapping of measurement error into the cloud property parameter space. An advantage of the optimal estimation approach, however, is that retrieval error can be quantified. From Table 1, retrieved optical depth is more accurate than retrieved effective radius for a given measurement error covariance. For example, assuming errors of 1.5 K in $T_{B,10.8}$, 2.5 K in ΔT_B, and 2 K in T_c, retrieved optical depths are accurate to approximately 10%, whereas uncertainties in retrieved effective radius are, on average, 35%. This result is explained by more careful examination of the physics underlying the retrieval. Optical depth is determined primarily by the $T_{B,10.8}$ measurement, whereas effective radius is heavily dependent on ΔT_B. An error of a few Kelvin in a $T_{B,10.8}$ measurement of 250 K amounts to an uncertainty of ~1% while a similar error in a ΔT_B measurement of 6 K corresponds to ~50% uncertainty. The result is substantially less inherent error in the optical depth estimate. These considerations also explain the fact that, while retrieved optical depths are very sensitive to the accuracy of the cloud thermodynamic temperature measurement regardless of the error in $T_{B,10.8}$ and ΔT_B, retrieved effective radii are not. Since uncertainties in optical depth due to errors in $T_{B,10.8}$ and ΔT_B are small, its accuracy is dictated by the error in T_c. As a result, optical depth estimates improve significantly for all curves as σ_{Tc} is reduced. Retrieved effective radii, however, are much more strongly dependent upon the error in $T_{B,10.8}$ and ΔT_B. If these errors are too large, the retrieval improves little regardless of the accuracy in cloud thermodynamic temperature.

[33] It should be noted that, while the numerical values quoted in Table 1 apply only to the specific combination of optical depth, effective radius, and cloud temperature con-

Table 1. Optical Depth and Effective Radius From Selected Synthetic Retrievals[a]

$(\sigma_{\Delta T_B},\sigma_{T_{B,10.8}})$	σ_{Tc}	Number	τ	r_e (μm)	A_τ	A_{re}
(0.5,0.5)	2.0	4944	0.80	14.24	1.00	0.99
	5.0	4953	0.81	14.16	1.00	0.99
	10.0	4931	0.83	13.91	1.00	0.94
	18.0	4877	0.85	13.50	0.99	0.92
	25.0	4833	0.87	13.25	0.99	0.88
(1.5,2.5)	2.0	4948	0.80	15.54	1.00	0.94
	5.0	4912	0.81	15.45	1.00	0.93
	10.0	4877	0.83	15.16	1.00	0.93
	18.0	4854	0.86	14.66	0.99	0.86
	25.0	4803	0.87	14.36	0.99	0.82
(3.0,5.0)	2.0	4875	0.81	16.51	1.00	0.75
	5.0	4867	0.82	16.42	1.00	0.75
	10.0	4860	0.84	16.10	0.99	0.73
	18.0	4788	0.87	15.56	0.99	0.70
	25.0	4731	0.92	15.24	0.98	0.67

[a]In all cases, synthetic measurements assuming an optical depth of 0.8, an effective radius of 14 μm, and a cloud thermodynamic temperature of 225 K were used. A priori initial guesses of $\tau = 1.5$, $r_e = 20$ μm, and $T_c = 235$ K were used in all cases. All standard deviations, denoted σ, are in K. Number indicates the number of convergent retrievals out of the 5000 random perturbations of the measurement vector for the given error combinations.

Table 2. Description of Each of the Eight Synthetic Retrieval Cases

	Case 1	Case 2	Case 3	Case 4	Case 5	Case 6	Case 7	Case 8
τ	0.8	1.8	0.8	1.8	0.8	1.8	0.8	1.8
r_e (μm)	14	14	14	14	22	22	22	22
T_c (K)	225	225	245	245	225	225	245	245

sidered, results for other sets of cloud properties are qualitatively similar. To illustrate this, synthetic retrievals were also performed for the eight combinations of optical depth, effective radius, and cloud temperature summarized in Table 2. In each case $\sigma_{\Delta TB}$ and $\sigma_{T_{B,10.8}}$ were assumed to be 1.5 and 2.5 K, respectively, consistent with the accuracy of the corrected two-layer model and under the assumption of spherical particles which obey a modified gamma distribution. Results for optical depth and effective radius are summarized in Tables 3 and 4, respectively.

[34] General trends in each of these synthetic cases agree with those described above, but the precise magnitude of retrieval errors is case dependent. Again, a physical understanding of the retrieval suggests that some combinations of measurements will have larger errors than others. Consider again the theoretical arches presented in Figure 1. Errors are large in cases where small changes in ΔT_B or $T_{B,10.8}$ result in large changes in retrieved properties. For example, at a cloud thermodynamic temperature of 255 K, very small differences in ΔT_B separate effective radii of 15 and 25 μm. In that case, small errors in the measurement vector will lead to very large errors in the retrieved effective radius. Similarly, errors are small when the measurement vector is located such that random error in the measurements does not change the retrieved parameters. In other words, retrieval uncertainties reflect the sensitivity of the retrieved parameters to the observations being used to retrieve them. As with most retrievals, the best results are obtained when the forward model is very sensitive to the retrieval parameters.

4.2. Nauru Retrievals

[35] Although synthetic retrievals provide useful information on algorithm performance, their validity rests entirely on the assumptions used in the numerical experiments. Physical measurements provide a much more rigorous and realistic means to examine algorithm performance. In this subsection, infrared radiances from the VIRS instrument aboard TRMM are combined with cloud boundary information from the ARM Nauru field site to determine both advantages and disadvantages of the algorithm when applied in real-world situations.

[36] The technique has been applied to all TRMM overpasses of Nauru Island (0.5°S and 166.9°E) from July to December 1999 yielding 23 thin cirrus cases. Figure 6 shows the $T_{B,10.8}$, ΔT_B, and precipitation fields for one such case which took place on the morning of 11 July 1999. Nauru is located in the center of each field just north of the central cold $T_{B,10.8}$ band. The $T_{B,10.8}$ and ΔT_B values of 269 and 5.5 K, respectively, suggest the presence of cirrus clouds likely forming from the detrainment of ice from the convective cells, visible in the corresponding precipitation field. Figure 7 shows the retrieved optical depth, effective radius, and cloud temperature for this case using a climatological estimate of cloud thermodynamic temperature determined by matching VIRS 10.8 μm brightness temperatures to the TRMM precipitation product 2A12 [*Kummerow and Giglio*, 1994]. Assuming that cirrus clouds were formed from outflow near the top of tropical convective cells, a mean and standard deviation of T_c as a function of latitude are calculated by averaging $T_{B,10.8}$ values in regions where precipitation rate was greater than 5 mm h^{-1} and $T_{B,10.8}$ was sufficiently low to indicate the presence of convection. The resulting cirrus cloud thermodynamic temperature for Nauru in the month of July is 218 ± 18 K. Figure 7 shows regions of thin cirrus clouds surround areas of convection, often exhibiting a smooth gradient with large values near convection tapering off to near zero further away. Retrieved effective radii are small, agreeing with the notion of large crystals settling out during detrainment [*Prabhakara et al.*, 1988]. Another interesting feature in these results is the fact that although the error in the climatological estimate of T_c is quite large and despite the uniform initial guess employed over the entire orbit swath, the cloud temperature field exhibits fine-scale structure. This is due to the use of T_c as a dynamic variable in the algorithm which allows the cloud thermodynamic temperature estimate to adjust through the heavy influence of the $T_{B,10.8}$ measurements in the Kernel matrix, **K**.

[37] While the potential for global observations afforded by satellites is clear, the lack of explicit cloud boundary information in the TRMM observations alone restricts the remainder of this study to the 23 cirrus clouds found directly over Nauru Island while we await the launch of future satellite missions. For each case cloud boundary information

Table 3. Bias and Random Error in Retrieved Optical Depth From Each of the Synthetic Retrieval Cases Summarized in Table 2[a]

	σ_{Tc} (K)	Case 1	Case 2	Case 3	Case 4	Case 5	Case 6	Case 7	Case 8	Avg.
Bias Error	2.0	0.4	0.6	0.4	1.0	0.6	1.5	1.1	3.3	1.1
	5.0	1.2	0.9	0.8	2.1	1.9	3.7	2.6	1.6	1.9
	10.0	3.7	1.7	1.4	6.6	6.0	6.1	6.0	1.2	4.1
	18.0	7.3	2.4	1.0	10.1	12.6	8.1	7.7	2.9	6.5
Random Error	2.0	9.3	14.2	13.3	25.1	9.3	15.1	13.5	27.0	15.8
	5.0	12.0	21.6	18.8	34.3	12.2	25.0	19.7	37.7	22.6
	10.0	20.4	29.7	32.5	40.6	21.9	35.5	36.9	45.1	32.8
	18.0	35.4	35.2	45.0	43.8	39.2	42.0	53.6	49.2	42.9

[a]Bias error indicates the percentage difference between the mean retrieved optical depth and the true optical depth. Random error is defined as the standard deviation over all retrievals divided by the mean of the retrieved optical depth for all convergent pixels, expressed as a percent.

Table 4. As in Table 3 But for Retrieved Effective Radius (μm)

	σ_{Tc} (K)	Case 1	Case 2	Case 3	Case 4	Case 5	Case 6	Case 7	Case 8	Average
Bias Error	2.0	8.6	19.9	12.5	18.2	2.0	3.3	2.9	13.7	10.1
	5.0	7.9	22.5	12.6	27.1	0.8	5.0	3.6	9.8	11.1
	10.0	5.6	26.5	13.4	38.8	2.5	7.0	4.8	4.7	12.9
	18.0	2.0	29.0	17.8	47.8	7.9	9.3	4.5	1.8	15.0
Random Error	2.0	34.9	72.1	52.6	95.1	40.6	56.8	48.6	66.3	58.4
	5.0	36.5	83.3	55.0	103	41.3	63.0	49.8	70.7	62.8
	10.0	41.8	99.0	62.6	112	43.9	71.5	53.9	75.7	70.0
	18.0	53.0	112	72.8	120	49.9	78.0	59.8	79.8	78.1

was determined by use of the ARM-derived cloud boundary product based on a combination of millimeter wavelength cloud radar, ceilometer, and lidar data. (Nauru data is obtained from the ARM program website: www.arm.gov.) Figure 8 shows the vertical distribution of thin cirrus clouds over Nauru for the day of the TRMM orbit case shown in Figures 6 and 7. Cloud temperature was determined by relating these cloud boundaries to temperature profiles determined from ARM sonde data. Microphysical parameters over Nauru using explicit cloud boundary information are compared to a retrieval using the less accurate climatological estimate of T_c in Figure 9.

[38] The most obvious feature in the results is the presence of two distinct clusters of points. While application of the current approach in the absence of explicit cloud boundary information indicates the presences of cirrus clouds in all cases, more careful examination of the ARM data suggests that the satellite actually observed a combination of cirrus and low-level water clouds in a number of scenes (denoted by diamonds) and pure liquid clouds (open boxes). The presence of the low-level clouds effectively changes the right foot of the arch to $T_{B,10.8}$ and ΔT_B values characteristic of the underlying clouds rather than the clear-sky atmosphere causing spurious results. In an operational retrieval, use of lidar to define cloud boundaries would provide a means to immediately discard such ambiguous cases.

[39] Retrieved optical depth and effective radius from the two retrievals exhibit reasonable agreement for the thin cirrus cases (open circles). Relative differences are larger for effective radius (~30%) than for optical depth (~10%), in agreement with differences in the sensitivity of the measurements to each. For the pure water cloud cases (open boxes), differences in retrieved properties are large because the estimates of T_c are significantly different. In one case, effective radius changes from 22 to 11 μm and the optical depth from 0.35 to 0.83 in the presence of explicit T_c information. Therefore, even if the algorithm were applicable in the case of a thin, low-level cloud, uncertainties in T_c will result in significant retrieval biases in the absence of cloud boundary information.

[40] The plot in the upper right of Figure 9 compares optical depth retrieval error from both retrievals. Retrieval error as defined in (3) is a function of both measurement error and the sensitivity of the model to retrieved parameters. For the ice cloud cases, error in retrieved optical depth is significantly smaller when explicit cloud boundary information is used relative to the TRMM climatology case. In the cases with water cloud contamination, however, error appears larger in the presence of explicit cloud boundary information. This is an artifact of the increased model sensitivity in the presence of large optical depth and small effective radii. As seen from Figure 1, small changes in effective radius and optical depth have little effect on $T_{B,10.8}$ and ΔT_B near the bottom of the arches but have a large effect near the top. Thus the apparent increase in error when ARM cloud boundary product is used result from the fact that optical depths are larger and effective radii smaller than in the TRMM climatology case.

[41] Finally, agreement between the retrieved cloud temperatures is poor in general. With the exception of the single optically thick cirrus cloud, T_c's are limited to near the climatological mean of 218 K in the TRMM climatology retrievals, whereas the ARM cloud boundary cases remain close to the measured T_c. Again, it is the striking difference between the two initial estimates of T_c that cause the differences in the other plots.

4.3. Implications for Studying Cloud–Radiation–Climate Interactions

[42] Estimates of the microphysical and optical properties of cirrus clouds, make it possible to study their impact on climate through their interactions with solar and terrestrial radiation. Cirrus clouds both warm the atmosphere by trapping longwave radiation emitted by the Earth's surface and cool it by reflecting incoming solar radiation. Their net effect on the environment is determined by the relative magnitudes of these two processes, which depend, in turn, on the absorption and emission properties of the constituent cloud particles. The goal of all space-based cirrus cloud microphysical retrievals is to constrain these quantities through direct estimation of the size and concentration of these particles.

[43] To estimate the impact of explicit cloud boundary information in studying the role of cirrus in the radiation budget, a number of the Nauru retrievals have been used in broadband radiative transfer calculations. Ice water path (IWP) derived from retrieved 10.8 μm optical depths, retrieved effective radii, and cloud height estimated from retrieved cloud thermodynamic temperature were used as input to the BUGSrad broadband radiative transfer model to calculate upwelling and downwelling longwave and shortwave fluxes at the TOA and surface (SFC). The BUGSrad model, which is currently implemented in the CSU general circulation model, employs the δ two-stream approximation to the radiative transfer equation [*Stephens and Webster*, 1979; *Ritter and Geleyn*, 1992; *Stephens et al.*, 2001a] over six shortwave and twelve longwave spectral bands. The model, explicitly accounts for the effects of scattering, absorption and emission from liquid and ice clouds using the parameterization of cloud optical properties introduced

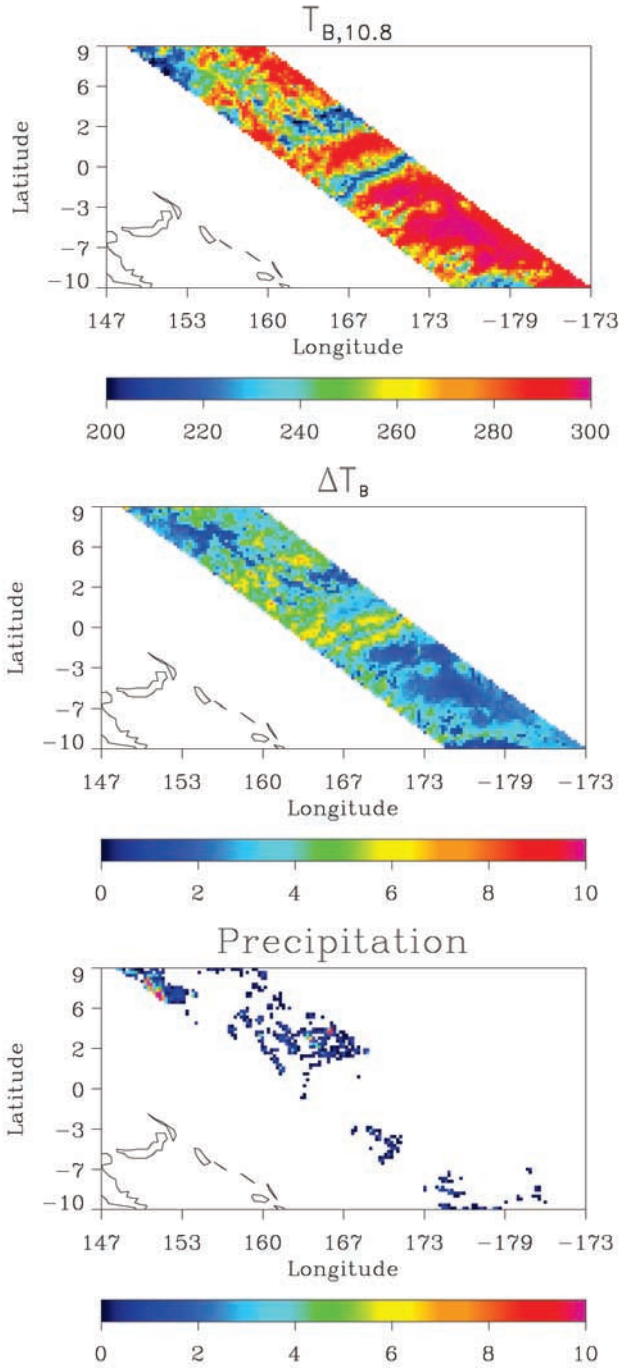

Figure 6. $T_{B,10.8}$ (in K), ΔT_B (in K), and precipitation fields (in mm h^{-1}) for a TRMM overpass of Nauru island on 11 July 1999. Nauru is located in the center of each field at 0.5°S and 166.9°E.

by *Stephens et al.* [1990], and includes gaseous absorption through the correlated k-distribution method of *Fu and Liou* [1992]. In the present application, atmospheric temperature and humidity profiles are assumed to follow the McClatchey tropical atmosphere and the all calculations are made at local noon for simplicity.

[44] Results are summarized for three cases in Table 5 chosen to be representative of a number of different scenes to which space-based measurements are likely to be applied. The first case, observed on 11 July 1999, corresponds to a high, thin cirrus cloud, ideally suited for retrievals making use of split-window radiances. The second case, occurring later that day, consists of another high cirrus cloud but one that is approximately 4 times thicker than the first near the upper limit of optical thickness for which meaningful results can be obtained using this technique. The final case is a

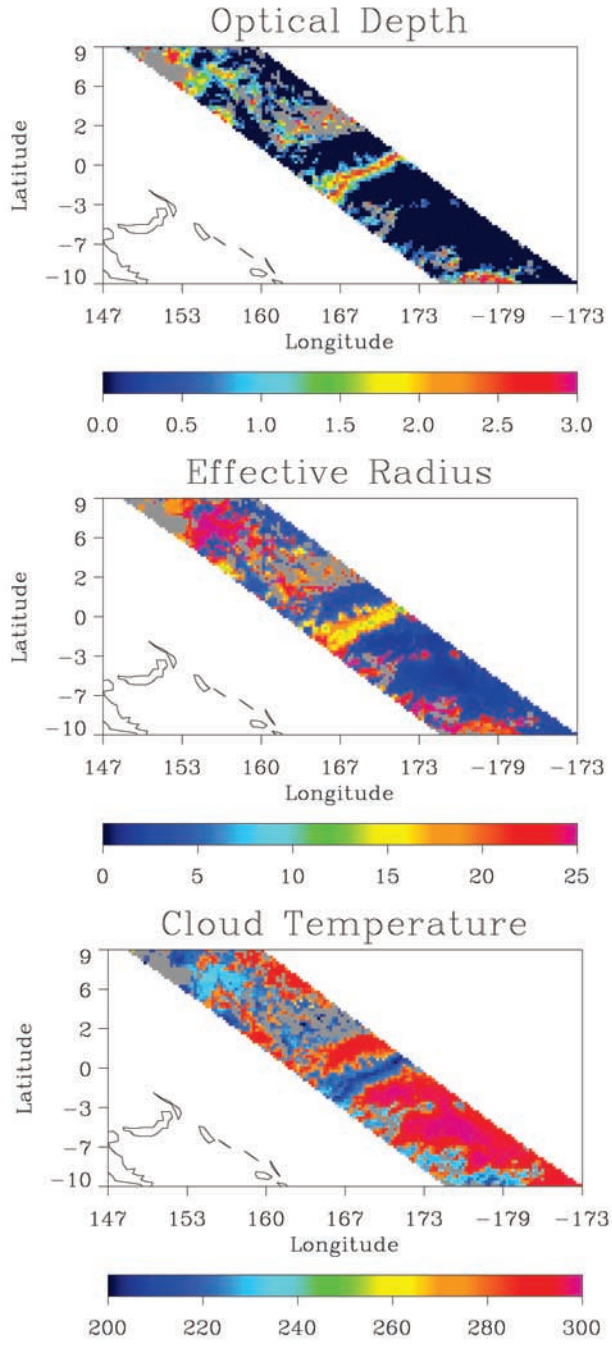

Figure 7. Retrieved optical depth, effective radius (in μm), and cloud thermodynamic temperature (in K) using TRMM climatology estimate of cloud temperature for the TRMM orbit in Figure 6. Gray pixels represent areas of optically thick, precipitating cloud.

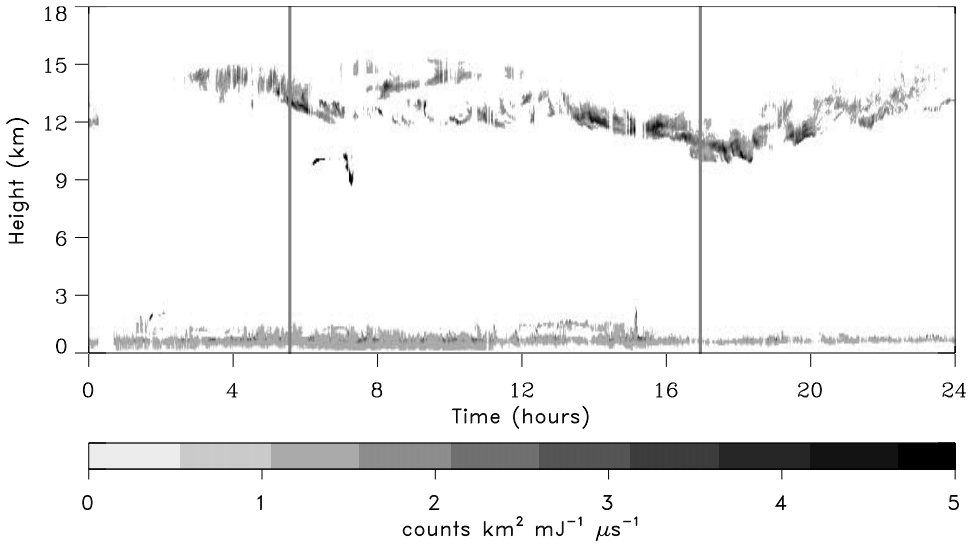

Figure 8. The normalized corrected relative backscatter from micropulse lidar located at the ARM site on Nauru. The two gray lines indicate the times of TRMM overpasses and the morning overpass corresponds to the observations and retrieval results shown in Figures 6 and 7.

much lower cloud with an emitting temperature near 260 K. By virtue of its altitude, this cloud is likely composed of liquid droplets but this information is difficult to determine using window radiances alone increasing the probability of misinterpreting it as a thin cloud in the absence of explicit cloud boundary information.

[45] In each of the first two cases cloud thermodynamic temperatures derived from the ARM cloud boundary prod-

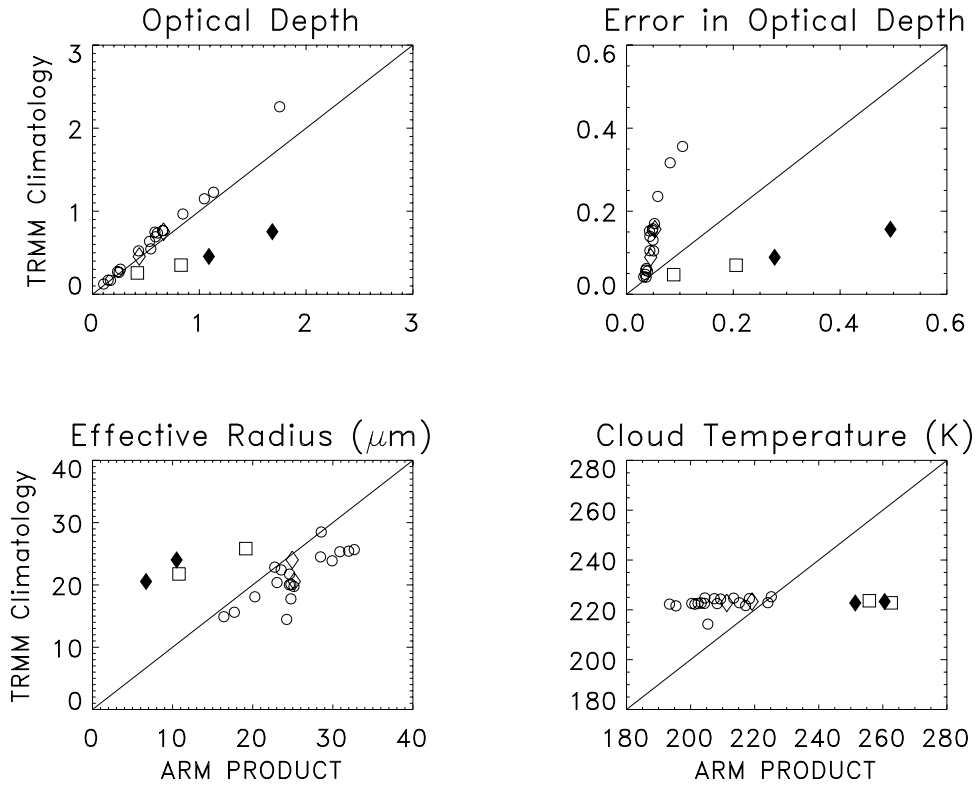

Figure 9. Scatterplots of retrieved optical depth, effective radius (in μm), cloud temperature (in K), and error in optical depth using estimates of cloud temperature from TRMM climatology versus that from the ARM cloud boundary product. Open circles represent thin cirrus clouds. Open boxes represent water clouds. Open diamonds and filled diamonds represent cirrus clouds and water clouds, respectively, for cases where the satellite field of view was filled by both types of cloud at the same time. A one-to-one line has been plotted on each graph for reference.

Table 5. Broadband Radiative Fluxes (in W m^{-2}) From BUGSrad for Selected Nauru Ice Cloud Retrievals[a]

Date	ARM	$\tau_{10.8}$	r_e (μm)	T_c (K)	$F^{\uparrow}_{LW,TOA}$	$F^{\uparrow}_{SW,TOA}$	$F^{\downarrow}_{LW,SFC}$	$F^{\downarrow}_{SW,SFC}$
11 July 1999	No	0.52	20.0	223	186 ± 20	262 ± 6	418.7 ± 0.2	848 ± 7
11 July 1999	Yes	0.43	24.6	200	185 ± 8	259 ± 3	418.1 ± 0.1	851 ± 4
11 July 1999	No	2.3	14.5	214	112 ± 34	347 ± 99	420.5 ± 0.5	755 ± 96
11 July 1999	Yes	1.8	24.2	205	119 ± 11	320 ± 20	418.7 ± 0.2	781 ± 20
16 October 1999	No	0.35	21.8	223	200 ± 16	255 ± 5	418.2 ± 0.1	856 ± 5
16 October 1999	Yes	0.83	10.8	263	207 ± 10	277 ± 13	422.6 ± 0.7	831 ± 14

[a]Horizontal lines delineate the three cases investigated. Two sets of fluxes are computed for each case, corresponding to retrievals without (upper set) and with (lower set) explicit cloud boundary information, respectively. Uncertainties, denoted by ±X, are estimated by perturbing retrieved cloud properties by their errors as established in the estimation process.

uct both modify the magnitude and increase the accuracy of all fluxes. Uncertainties are decreased by a factor of 2 in the thin cirrus case and three to four in the presence of the thicker cloud. Furthermore, in the absence of cloud boundary information, retrieved T_c's are generally close to the initial guess of 218 K failing to reflect large differences in vertical boundaries of the three cases. As a result, the vertical placement of the cloud heating in the atmosphere is poorly constrained in these retrievals which can have serious consequences in modeling global circulations [e.g., *Hartmann et al.*, 1984; *Lau and Peng*, 1987].

[46] In the third case, fluxes appear to be better constrained in the absence of cloud boundary information. This is deceiving since the cloud is likely actually a liquid cloud scene to which the retrieval should not be applied. In this case, to match the 10.8 and 12 μm radiances observed by TRMM the algorithm creates an equivalent thin ice cloud consisting of 22 μm particles and emitting at 223 K. Explicit cloud boundary information results in a much thicker cloud consisting of 11 μm particles but emitting at a more appropriate 263 K. Since the radiative fluxes are most sensitive to small changes in effective radius when particles are small to begin with, their uncertainties are largest when cloud boundaries are constrained. Operationally, however, the presence of cloud boundary information allows the algorithm to flag this scene as a possible liquid cloud while its absence could lead to the very serious error of a complete misclassification.

[47] It is important to note that, in all three cases, cloud boundary information has little influence on downwelling longwave radiation at the Earth's surface. This reflects the fact that downwelling radiation at the surface is due to emission from water vapor in the moist tropical atmosphere. Conversely, increased reflection of incoming solar radiation to space directly reduces downwelling shortwave radiation incident at the surface thus the errors in the two shortwave fluxes are strongly correlated.

[48] Considering the fact that approximately a third of the planet is covered by cirrus at any given time [*Liou*, 1986], one can imagine the impact of such errors when integrated on large scales. The potential increase in accuracy afforded by the combination of explicit cloud boundary information and infrared observations is very promising in light of these considerations. For example, assuming cirrus cloud retrieval errors lead to average uncertainties in longwave fluxes at TOA of ~30 W m^{-2}, the absence of cloud boundaries leads to errors in global estimates of outgoing longwave radiation (OLR) as large as 10 W m^{-2}. In practice the random component of this uncertainty will be substantially reduced in the averaging process but we have no way of separating systematic and random errors at this time. Explicit estimates of cloud boundaries reduce average TOA longwave flux uncertainties to ~10 W m^{-2} and corresponding global OLR errors to ~3 W m^{-2}. For comparison purposes, the magnitude of the global-mean radiative effects of aerosols (both direct and indirect) are expected to be on the order of 1–2 W m^{-2} while the longwave radiative signature of atmospheric CO_2 is ~1.5 W m^{-2} [*IPCC*, 1995]. Clearly, improved estimates of ice cloud microphysical and optical properties afforded by including explicit cloud boundary information are critical to the problem of establishing observational evidence for climate variability resulting from anthropogenically induced changes in either of these two important atmospheric constituents.

5. Conclusions

[49] An optimal estimation algorithm that combines explicit cloud boundary information with the split-window approach to estimate the microphysical properties of thin cirrus clouds has been introduced. The inclusion of explicit

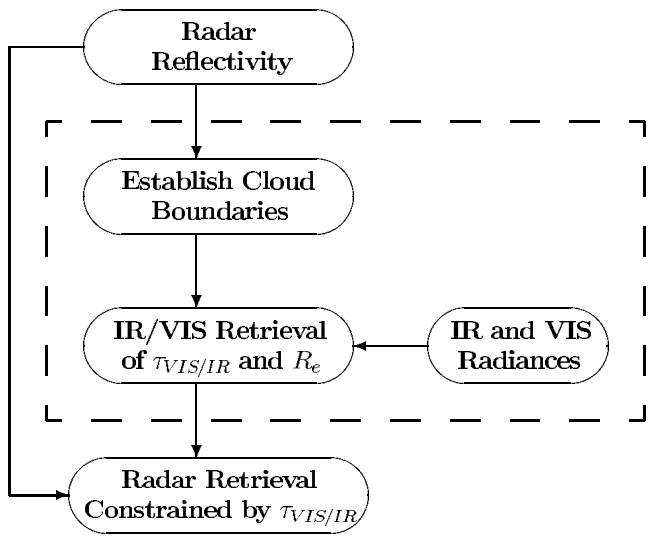

Figure 10. Schematic representation of a methodology for retrieving vertical distributions of cirrus cloud microphysical properties from a combination of active and passive observations. The elements of the approach that are explicitly addressed in this paper are highlighted with the dashed box.

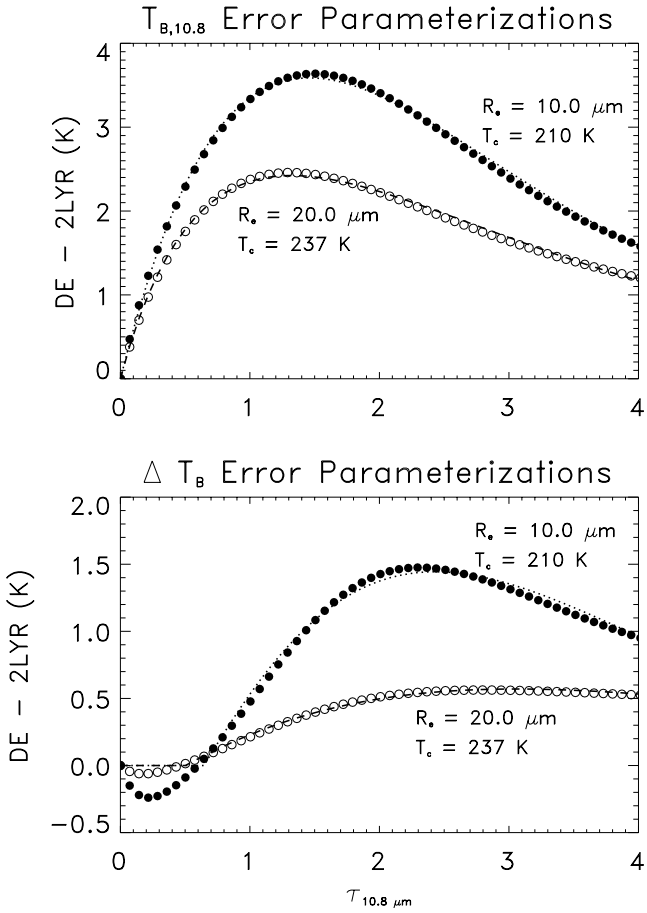

Figure A1. Differences in 10.8 μm brightness temperature and ΔT_B between the two-layer and the DE radiative transfer models. Computed model differences for an assumed effective radius of 10 μm and a cloud thermodynamic temperature of 210 K are represented by filled circles while open circles correspond to an effective radius of 20 μm and a cloud thermodynamic temperature of 237 K. Fits to these data using the expression in (A1) are illustrated but the dotted and dashed curves, respectively.

cloud boundary information is found to significantly reduce the biases inherent in traditional implementations of the of the approach. Furthermore, the optimal estimation framework provides error diagnostics for all retrieved parameters often lacking in other retrievals and facilitates addition of information from complementary sensors into the retrieval. *Ackerman et al.* [1990], for example, show that 8.5 μm radiances can be used in conjunction with those at window wavelengths to distinguish between water and ice clouds. Such information can easily be added to the algorithm providing a thermodynamic phase cloud mask, increasing its speed and accuracy when applied on global scales. In principle, a retrieval of cirrus properties could be performed from any data set that includes a direct estimate of cloud thermodynamic temperature, T_c, using the forward model developed here.

[50] Synthetic retrievals indicate that the more accurate the estimate of T_c, the higher the probability of obtaining an accurate retrieval given a measurement with random error. Retrieval errors provided by the optimal estimation approach suggest that optical depth is determined significantly more accurately than effective radius, an artifact of the sensitivity of the forward model physics to each of these parameters. For an error in cloud temperature of 2 K, characteristic of lidar-based estimates of cloud thermodynamic temperature, the average error in retrieved optical depth and effective radius are ~15 and ~60 percent, respectively, significantly better than retrievals performed with less accurate cloud temperature information. Application of the algorithm to coincident measurements of infrared radiances from TRMM and cloud boundary measurements from the ARM Nauru site confirms these results. Differences between retrievals using accurate cloud boundary information and those performed with a less accurate climatological estimate of T_c were on the order of 10 and 30 percent for optical depth and effective radius, respectively, while retrieval uncertainties were generally much larger in the absence of cloud boundary information. Furthermore, cloud boundary information proves invaluable in eliminating the potential for ambiguities in cases where the satellite field of view observed either multiple cloud layers or water clouds.

[51] If one third of the planet is assumed to be covered by cirrus clouds at any given time, the absence of cloud boundaries in the present work leads to errors in global estimates of OLR as large as 10 W m^{-2}. Accurate estimates of cloud boundaries are found to reduce global OLR errors to ~3 W m^{-2}. When compared to IPCC estimates of the global-mean radiative effects of aerosols (1–2 W m^{-2}) and CO_2 (~1.5 W m^{-2}) it is clear that improved estimates of ice cloud microphysical and optical properties afforded by including explicit cloud boundary information are critical to the problem of establishing observational evidence to constrain the climatic impact of either of these highly variable atmospheric constituents.

[52] Colocated active and passive measurements will soon be available on a global scale with coincident measurements from the Earth Observing System (EOS) Aqua, CALIPSO, and CloudSat satellites which are scheduled to fly in formation in early 2004. Infrared radiances from the

Table A1. Parameters Used to Correct 10.8 μm Brightness Temperatures[a]

	T_c = 195 K			T_c = 210 K			T_c = 224 K			T_c = 237 K			T_c = 250 K		
R_e	A	B	τ_n	A	B	τ_n	A	B	τ_n	A	B	τ_n	A	B	τ_n
5	4.99	1.67	2.36	6.14	1.36	2.07	5.94	1.80	1.25	6.24	1.13	1.60	6.01	1.06	1.44
10	4.66	1.28	1.74	6.08	1.09	1.60	6.12	1.01	1.37	6.62	0.94	1.23	6.55	0.89	1.12
15	4.20	1.11	1.46	5.64	0.97	1.42	5.77	0.91	1.21	6.33	0.87	1.12	6.37	0.83	1.02
20	3.77	1.02	1.31	5.08	0.93	1.39	5.25	0.88	1.18	5.84	0.85	1.11	5.96	0.82	1.02
25	3.43	0.97	1.24	4.63	0.92	1.42	4.82	0.87	1.20	5.43	0.84	1.14	5.61	0.82	1.04

[a]Effective radius, R_e, is in μm.

Table A2. As in Table A1 But for 10.8–12 μm Brightness Temperature Differences[a]

	T_c = 195 K			T_c = 210 K			T_c = 224 K			T_c = 237 K			T_c = 250 K		
R_e	A	B	τ_n	A	B	τ_n	A	B	τ_n	A	B	τ_n	A	B	τ_n
5	4.08	1.67	2.30	3.59	1.36	2.25	3.31	1.25	2.10	3.25	1.13	1.91	2.77	1.06	1.95
10	1.47	1.28	2.65	1.58	1.09	2.35	1.43	1.01	2.32	1.26	0.94	2.46	1.20	0.89	2.41
15	0.82	1.11	2.60	0.86	0.97	2.49	0.78	0.91	2.58	0.77	0.87	2.63	0.72	0.83	2.76
20	0.49	1.02	2.78	0.63	0.93	2.37	0.51	0.88	2.87	0.51	0.85	3.01	0.50	0.82	3.17
25	0.42	0.97	2.47	0.52	0.92	2.34	0.41	0.87	2.98	0.36	3.57	0.84	0.37	3.69	0.82

[a]Effective radius, R_e, is in μm.

MODIS instrument aboard Aqua can be combined with lidar data from CALIPSO, or, equivalently, cloud radar data from the 94 GHz CPR, to retrieve thin cirrus clouds globally. The work presented here, for example, could be used in conjunction with a retrieval scheme developed by *Benedetti et al.* [2003] for an estimate of the vertical distribution of cloud microphysical properties, as depicted in Figure 10. An optical depth generated by the combination of active and passive measurements as described in this paper provides a constraint in the *Benedetti et al.* [2003] algorithm. The vertical distribution of both particle size and ice water content is then generated from the vertical profile of radar reflectivities observed by CloudSat initially used to supply cloud boundary information in the optical depth retrieval. Furthermore, provided suitable forward models are developed, information from the visible or near-infrared channels on MODIS can be incorporated to further augment the flexibility of the retrieval and increase its accuracy. The resulting climatology fits well within the objectives of all three missions offering the potential to significantly improve characterization of cirrus cloud extent and microphysical properties necessary to understand the physical processes underlying climate variability and change.

Appendix A: Bias Correction

[53] As noted in section 3.2, brightness temperatures computed using the two-layer radiative transfer model employed in the present study and the doubling adding model of *Deeter and Evans* [1998] do not agree perfectly. This is evident in Figure A1 which presents differences in modeled $T_{B,10.8}$ and ΔT_B are for two cirrus clouds with different emitting temperatures and effective radii. Given its simplicity, it is to be expected that our model may have some shortcomings relative to the more rigorous solution employed in the DE model. If uncorrected, however, these errors can lead to biases in retrieved cloud properties.

[54] In the interest of minimizing computation time while maximizing retrieval accuracy a correction has been developed to improve the agreement between the two models. In general, errors in modeled brightness temperatures decrease with increasing particle size and cloud thermodynamic temperatures. To capture this dependence, differences in $T_{B,10.8}$ and ΔT_B between the two models have been parameterized using the following expression

$$\delta = A\tau e^{-(\tau/\tau_n)^B} \tag{A1}$$

for a variety of cases spanning the range over which the retrieval is to be applied. Fits to the two cases illustrated in Figure A1 are represented by dotted and dashed lines and parameters for a wide range of effective radius and cloud thermodynamic temperature combinations are summarized in Tables A1 and A2. Operationally, given an effective radius, optical depth, and cloud thermodynamic temperature, the forward model proceeds as outlined in (6), (7), (8), and (9) but, prior to returning to the retrieval, $T_{B,10.8}$ and ΔT_B are corrected using (A1). Fit parameters are evaluated via linear interpolation between the values presented in Tables A1 and A2.

[55] **Acknowledgments.** We thank Ping Yang for his assistance in determining cloud particle absorption properties and Merritt Deeter and Frank Evans for allowing us to use their forward model for calibrating our own model. Angela Benedetti provided many useful insights into our problem. Finally, we thank each of the three anonymous reviewers for their thorough reviews and their helpful comments. Nauru data were obtained from the Atmospheric Radiation Measurement (ARM) Program sponsored by the U.S. Department of Energy, Office of Science, Office of Biological and Environmental Research, Environmental Sciences Division. Funding for this work was provided by NASA research grants NAS5-99237 (TRMM), NAS1-99103 (CALIPSO), and NAG5-7719 (CloudSat).

References

Ackerman, S., W. Smith, J. Spinhirne, and H. Revercombe, The 27–28 October 1986 fire ifo cirrus case study: Spectral properties of cirrus clouds in the 8–12 μm window, *Mon. Weather Rev.*, *118*, 2377–2388, 1990.

Austin, R., and G. Stephens, Retrieval of stratus cloud microphysical parameters using millimeter-wave radar and visible optical depth in preparation for CloudSat, *J. Geophys. Res.*, *106*, 28,233–28,242, 2001.

Baum, B., and B. Wielicki, Cirrus cloud retrieval using infrared sounding data: Multilevel cloud layers, *J. Appl. Meteorol.*, *33*, 107–117, 1994.

Benedetti, A., G. L. Stephens, and J. M. Haynes, Ice cloud microphysics retrievals from millimeter radar and visible optical depth using an estimation theory approach, *J. Geophys. Res.*, *108*, doi:10.1029/2002JD002693, in press, 2003.

Deeter, M., and K. Evans, A hybrid Eddington-single scattering radiative transfer model for computing radiances from thermally emitting atmospheres, *J. Quant. Spectrosc. Radiat. Transfer*, *60*, 635–648, 1998.

Dowling, D., and L. Radke, A summary of the physical properties of cirrus clouds, *J. Appl. Meteorol.*, *29*, 970–978, 1990.

Engelen, R., and G. Stephens, Infrared radiative transfer in the 9.6 μm band: Application to TOVS ozone retrieval, *J. Geophys. Res.*, *92*, 6929–6940, 1997.

Engelen, R., and G. Stephens, Characterization of water vapour retrievals from TOVS/HIRS and SSM/T-2 measurements, *Q. J. R. Meteorol. Soc.*, *125*, 331–351, 1999.

Eyre, J. R., G. A. Kelly, A. P. McNally, E. Anderson, and A. Persson, Assimilation of TOVS radiance information through one-dimensional variational analysis, *Q. J. R. Meteorol. Soc.*, *119*, 1427–1463, 1993.

Flatau, P., Scattering by irregular particles in anomalous diffraction and discrete dipole approximations, Ph.D. thesis, Colo. State Univ., Fort Collins, Colo., 1992.

Francis, P., A. Jones, R. Saunders, K. Shine, A. Slingo, and Z. Sun, An observational and theoretical study of the radiative properties of cirrus: Some results from ICE'89, *Q. J. R. Meteorol. Soc.*, *120*, 809–848, 1994.

Fu, Q., and K.-N. Liou, On the correlated k-distribution for radiative transfer in nonhomogeneous atmospheres, *J. Atmos. Sci.*, *49*, 2139–2156, 1992.

Fu, Q., M. Baker, and D. Hartmann, Tropical cirrus and water vapor: An effective Earth infrared iris feedback?, *Atmos. Chem. Phys.*, *2*, 31–37, 2002.

Grenfell, T., and S. Warren, Representation of a nonspherical ice particle by a collection of independent spheres for scattering and absorption of radiation, *J. Geophys. Res.*, *104*, 31,697–31,709, 1999.

Hartmann, D. L., H. H. Hendon, and J. R. A. Houze, Some implications of the mesoscale circulation in tropical cloud clusters for large-scale dynamics and climate, *J. Atmos. Sci.*, *41*, 113–121, 1984.

Inoue, T., On the temperature and effective emissivity determination of semi-transparent cirrus clouds by bi-spectral measurements in the 10 μm window region, *J. Meteorol. Soc. Jpn.*, *63*, 88–89, 1985.

IPCC, Intergovernmental Panel on Climate Change (IPCC) (1995) World Meteorological Office, United Nations Environmental Programme, *Radiative Forcing of Climate Change, The 1994 Report of the Scientific Assessment Working Group of IPCC, Summary for Policymakers*, Cambridge Univ., Cambridge U.K., 1995.

King, M., Y. Kaufman, W. Menzel, and D. Tanre, Remote sensing of cloud, aerosol, and water vapor properties from the Moderate Resolution Imaging Spectrometer (MODIS), *IEEE Trans. Geosci. Remote Sens.*, *30*, 2–27, 1992.

Kummerow, C., and L. Giglio, A passive microwave technique for estimating rainfall and vertical structure information from space, part 1, algorithm development, *J. Appl. Meteorol.*, *33*, 3–18, 1994.

Lau, K.-M., and L. Peng, Origin of low-frequency (intraseasonal) oscillations in the tropical atmosphere, part 1, Basic theory, *J. Atmos. Sci.*, *44*, 950–972, 1987.

L'Ecuyer, T., and G. Stephens, An estimation-based precipitation retrieval algorithm for attenuating radars, *J. Appl. Meteorol.*, *41*, 272–285, 2002.

Lindzen, R., M. Chou, and A. Hou, Does the Earth have an adaptive infrared iris?, *Bull. Am. Meteorol. Soc.*, *82*, 417–432, 2001.

Liou, K. N., Influence of cirrus clouds on weather and climate processes: A global perspective, *Mon. Weather Rev.*, *114*, 1167–1199, 1986.

Lyu, C., W. Barnes, and R. Barnes, First results from the on-orbit calibration of the Visible and Infrared Scanner for the Tropical Rainfall Measuring Mission, *J. Atmos. Oceanic Technol.*, *17*, 385–394, 2000.

Marks, C., and C. Rodgers, A retrieval method for atmospheric composition from limb emission measurements, *J. Geophys. Res.*, *98*, 14,939–14,953, 1993.

McClatchey, F. A., R. W. Fenn, J. E. Selby, F. E. Volz, and J. S. Goring, *Optical Properties of the Atmosphere*, 3rd ed., AFCRL-72-0497, 102 pp., Air Force Cambridge Res. Lab., Hanscom AFB, Mass., 1972.

Menzel, W., D. Wylie, and K. Strabala, Seasonal and diurnal changes in cirrus clouds as seen in four years of observations with the VAS, *J. Appl. Meteorol.*, *31*, 370–385, 1992.

Miller, S., G. Stephens, C. Drummond, A. Heidinger, and P. Partain, A multisensor diagnostic satellite cloud property retrieval scheme, *J. Geophys. Res.*, *105*, 19,955–19,971, 2000.

Mitchell, D., and W. Arnott, A model predicting the evolution of ice particle size spectra and radiative properties of cirrus clouds, part 2, Dependence of absorption and extinction on ice crystal morphology, *J. Atmos. Sci.*, *51*, 817–832, 1994.

Parol, F., J. Buriez, G. Brogniez, and Y. Fouquart, Information content of AVHRR channels 4 and 5 with respect to the effective radius of cirrus cloud particles, *J. Appl. Meteorol.*, *30*, 973–984, 1991.

Pierrehumbert, R., Thermostats, radiator fins, and the local runaway greenhouse, *J. Atmos. Sci.*, *52*, 1784–1806, 1995.

Prabhakara, C., R. Fraser, M. Wu, and R. Curran, Thin cirrus clouds: Seasonal distributions over oceans deduced from NIMBUS-4 IRIS, *J. Appl. Meteorol.*, *27*, 379–399, 1988.

Reist, P. C., *Aerosol Science and Technology*, McGraw-Hill, New York, 1993.

Ritter, B., and J.-F. Geleyn, A comprehensive radiation scheme for numerical weather prediction models with potential applications in climate simulations, *Mon. Weather Rev.*, *120*, 303–325, 1992.

Rodgers, C., Retrieval of atmospheric temperature and composition from remote measurements of thermal radiation, *Rev. Geophys. Space Phys.*, *14*, 609–624, 1976.

Rodgers, C., Characterization and error analysis of profiles retrieved from remote sounding measurements, *J. Geophys. Res.*, *95*, 5587–5595, 1990.

Rodgers, C., *Inverse Methods for Atmospheric Sounding*, World Sci. Publ., River Edge, N. J., 2000.

Rosenfield, J. E., D. B. Considine, M. R. Schoeberl, and E. V. Browell, The impact of subvisual cirrus near the tropopause on stratospheric water vapor, *Geophys. Res. Lett.*, *49*, 1883–1886, 1998.

Sassen, K., Cirrus: A modern perspective, in *Cirrus*, edited by D. K. Lynch et al., pp. 11–40, Oxford Univ. Press, New York, 2002.

Stephens, G. L., Radiative properties of cirrus clouds in the infrared region, *J. Atmos. Sci.*, *37*, 435–446, 1980.

Stephens, G. L., *Remote Sensing of the Lower Atmosphere*, Oxford Univ. Press, New York, 1994.

Stephens, G. L., Cirrus, climate, and global change, in *Cirrus*, edited by D. K. Lynch et al., pp. 433–448, Oxford Univ. Press, New York, 2002.

Stephens, G. L., and P. J. Webster, Sensitivity of radiative forcing to variable cloud and moisture, *J. Atmos. Sci.*, *36*, 1542–1556, 1979.

Stephens, G. L., and P. Webster, Clouds and climate: Sensitivity of simple systems, *J. Atmos. Sci.*, *38*, 235–247, 1981.

Stephens, G. L., S.-C. Tsay, J. P. W. Stackhouse, and P. J. Flatau, The relevance of the microphysical and radiative properties of cirrus clouds to climate and climatic feedback, *J. Atmos. Sci.*, *47*, 1742–1753, 1990.

Stephens, G. L., P. M. Gabriel, and P. T. Partain, Parameterization of atmospheric radiative transfer, 1, Validity of simple models, *J. Atmos. Sci.*, *58*, 3391–3409, 2001a.

Stephens, G. L., M. Vaughn, R. Engelen, and T. Anderson, Toward retrieving properties of the tenuous atmosphere using space-based lidar measurements, *J. Geophys. Res.*, *106*, 28,143–28,157, 2001b.

Wielicki, B., B. Barkstrom, E. R. L. Harrison III, G. Smith, and J. Cooper, Clouds and the earth's radiant energy system (CERES): An earth observing system experiment, *Bull. Am. Meteorol. Soc.*, *77*, 853–868, 1996.

Yang, P., B. Gao, B. Baum, Y. Hu, W. Wiscombe, S. Tsay, D. Winker, and S. Nasiri, Radiative properties of cirrus clouds in the infrared (8–13 μm) spectral region, *J. Quant. Spectrosc. Radiat. Transfer*, *70*, 473–504, 2001.

S. J. Cooper, T. S. L'Ecuyer, and G. L. Stephens, Department of Atmospheric Science, Colorado State University, Fort Collins, CO 80523, USA. (cooper@atmos.colostate.edu)